

Context-Aware Weakly Supervised Image Manipulation Localization with SAM Refinement

Xinghao Wang, Tao Gong*, Qi Chu, Bin Liu and Nenghai Yu

Abstract—Malicious image manipulation poses societal risks, increasing the importance of effective image manipulation detection methods. Recent approaches in image manipulation detection have largely been driven by fully supervised approaches, which require labor-intensive pixel-level annotations. Thus, it is essential to explore weakly supervised image manipulation localization methods that only require image-level binary labels for training. However, existing weakly supervised image manipulation methods overlook the importance of edge information for accurate localization, leading to suboptimal localization performance. To address this, we propose a Context-Aware Boundary Localization (CABL) module to aggregate boundary features and learn context-inconsistency for localizing manipulated areas. Furthermore, by leveraging Class Activation Mapping (CAM) and Segment Anything Model (SAM), we introduce the CAM-Guided SAM Refinement (CGSR) module to generate more accurate manipulation localization maps. By integrating two modules, we present a novel weakly supervised framework based on a dual-branch Transformer-CNN architecture. Our method achieves outstanding localization performance across multiple datasets.

Index Terms—Image Manipulation Localization, Weakly Supervised, Context-Aware Boundary Localization

I. INTRODUCTION

WITH the proliferation of maliciously forged images, the localization of manipulated regions has become critical for combating misinformation. Currently, most image manipulation localization methods leverage both image-level binary classification labels and pixel-level mask annotations for fully supervised training [1], [2]. Early approaches leveraged noise, boundaries, and color inconsistencies [3], [4], while recent methods focus on content-agnostic features: CAT-Net [5] learns compression artifacts; MVSS-Net [6] uses multi-scale noise; Mantra-Net [7] detects operational boundaries; and PROMPT-IML [8] aligns semantic and high-frequency features via pre-trained models.

Despite significant advances in fully supervised image manipulation localization methods [1], [12], the growing diversity and complexity of manipulation techniques have made acquiring comprehensive pixel-level mask annotations increasingly impractical. Dense annotation of manipulated regions is both challenging and time-consuming. As a result, recent research has shifted towards weakly supervised approaches to enhance generalization and localization performance. For instance, WSCL [13] introduces multi-source consistency and inter-patch consistency modules by exploiting the self-consistency

properties of manipulated images. While effective for manipulation detection tasks, its localization performance is limited by inadequate consideration of boundary information, which is crucial for accurate manipulation localization.

Image manipulation techniques like copy-move [14], [15] and splicing [16] involve non-generative operations in which manipulated regions are copied from authentic areas. As a result, the noise and texture within manipulated regions often resemble those of real regions, making the boundaries of manipulated areas crucial for localization. To better learn boundary information, we propose a Context-Aware Boundary Localization (CABL) module that utilizes context-inconsistency at the boundaries to more precisely identify manipulated regions. Furthermore, previous methods [13], [17] in weakly supervised image manipulation localization have largely overlooked the potential of Class Activation Mapping (CAM) [18]. In our approach, we compute CAM maps using the output of a dual-branch Transformer-CNN network to generate coarse masks of manipulated regions. To refine these coarse masks, we leverage the strong capabilities of the Segment Anything Model (SAM) [19] through a CAM-Guided SAM Refinement (CGSR) module. Specifically, we use the bounding rectangle of the largest connected component from the coarse masks and the positive and negative sampling points from the CAM [18] without maximum-minimum normalization as visual prompts for SAM [19]. SAM [19] can generate more accurate localization masks using these visual prompts, without requiring additional training. By integrating these two modules, we propose a novel framework that combines CABL and CGSR within a dual-branch Transformer-CNN architecture. This framework can learn the context-inconsistency of the manipulated images under weakly supervised training conditions, enabling precise localization of the manipulated regions.

Experiments validate that our method achieves state-of-the-art performance in both manipulation detection and localization, effectively identifying and segmenting manipulated regions across diverse scenarios. The principal contributions of this work include:

- (1) We propose the **Context-Aware Boundary Localization (CABL) module** that explicitly learns context-inconsistency at manipulated boundaries, enabling precise localization of manipulated regions.
- (2) We propose the **CAM-Guided SAM Refinement (CGSR) module**, employing CAM [18] to generate the coarse-grained masks and achieving more precise localization results base on SAM’s [19] powerful segmentation capabilities without additional training.
- (3) We train the model using only image-level binary clas-

* Corresponding author: tgong@ustc.edu.cn.

The authors are with the University of Science and Technology of China, Hefei 230026, China. (e-mail: {wxhwxhwxh}@mail.ustc.edu.cn, {tgong, qchu, flowice, ynh}@ustc.edu.cn).

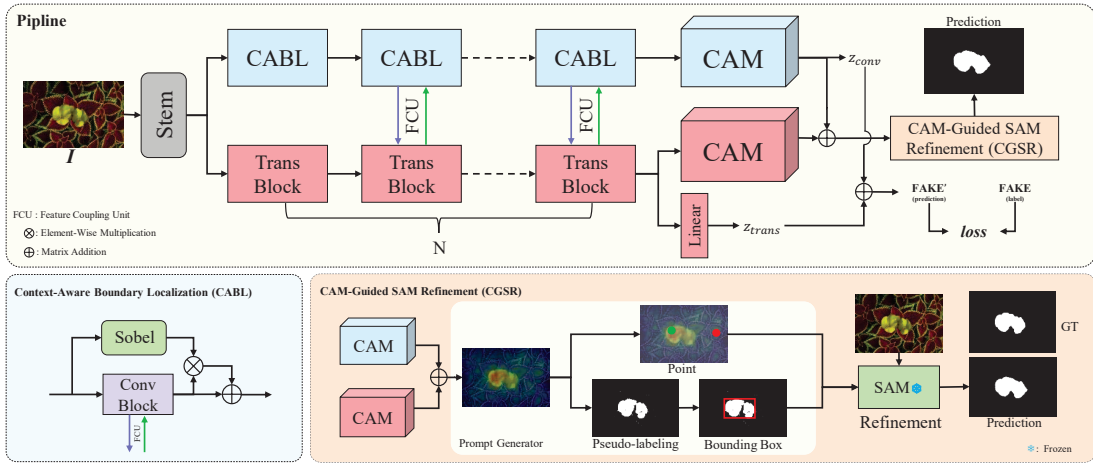


Fig. 1: The framework of our method: We integrate our custom-designed CABL module and CGSR module into the backbone. We train the model using only images and image-level binary labels. Sobel [9] denotes the Sobel operator, Stem generates patch embeddings, ConvBlock and TransBlock [10] are composed of convolution layers and transformer [11] layers respectively. The green point in the Prompt Generator indicates the positive point prompt, the red point represents the negative point prompt, and the red box denotes the bounding box prompt.

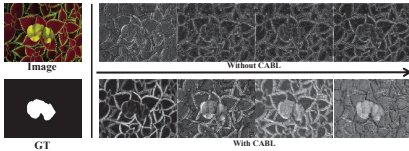


Fig. 2: Right of vertical line: first row (w/o CABL) shows feature maps of first 4 blocks; second row (w/ CABL) shows enhanced maps. Arrows indicate deeper block directions.

sification labels from the CASIAv2 [20] dataset and evaluate its performance on four unseen test datasets, demonstrating its effectiveness.

II. METHODOLOGY

A. Overview

As shown in Fig.1, the framework first processes the input image through a Stem module to extract hierarchical features, followed by two parallel branches: N-block CABL module explicitly modeling boundary context-inconsistency for manipulation localization, and TransBlock [10] capturing global semantic features via self-attention. The two branches use the Feature Coupling Unit (FCU) [27] to integrate local and global features. Classification is supervised with Binary CrossEntropy Loss (BCE) [28]. The final layer of each branch undergoes global average pooling, and the results are weighted to generate the Class Activation Map (CAM) [18] for each class (Sec.II-B). These coarse-grained masks are then used to create prompts. The prompts are subsequently input into the Segment Anything Model (SAM) [19] for refinement, yielding final localization predictions without additional training (Sec.II-C).

B. Context-Aware Boundary Localization (CABL)

Image manipulation tasks such as copy-move [14], [15] and splicing [16] typically involve regions sourced from genuine images where internal textures and noise are similar to real regions, the localization model must focus on boundary areas between real and manipulated regions. However, weakly supervised methods face challenges in this context, as they

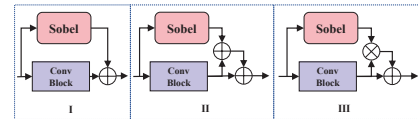


Fig. 3: Originally designed for three possible CABL structures, structure III was eventually used as CABL

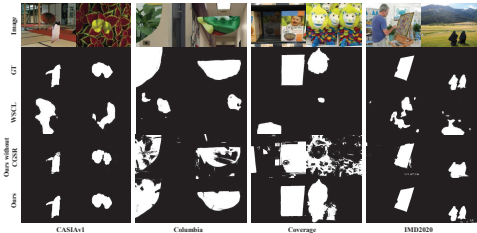


Fig. 4: Qualitative results on four datasets. From top to bottom: Image, GT, WSCL+MIL-FCN, Ours w/o and w/ SAM [19] refinement.

rely solely on image-level binary labels and cannot utilize pixel-level masks, complicating direct boundary learning. To address this, we propose utilizing non-learnable edge detection operators to extract high-frequency boundary information, which enhances the model’s focus on edge features.

The Context-Aware Boundary Localization (CABL) module is designed to capture context-inconsistent boundary information within feature maps. At each block, CABL extracts contextual features, applies an edge detection operator to amplify high-frequency boundary signals, and performs element-wise multiplication and residual connections [29] between boundary and image features. This aggregated boundary information is propagated through subsequent blocks. We adopt the Sobel operator [9] as the edge detector due to its computational efficiency and noise suppression capability. While the Prewitt operator [9] shares a similar design, it underperforms in noise robustness (Sec.III-D4). The CABL structure is illustrated in Fig.2, and its feature computation is formalized as:

$$F_i = S(F_{i-1}) \otimes C(F_{i-1}) \oplus C(F_{i-1}) \quad (1)$$

where F_i represents the features at the i -th block, $S(\cdot)$ extracts boundary features via Sobel filtering [9], $C(\cdot)$ represents con-

TABLE I: Comparison of Image Manipulation Detection and Localization Methods across Different Datasets^{1,2}

	Method	CASIaV1		Columbia		Coverage		IMD2020		Average	
		I-AUC	P-F1	I-AUC	P-F1	I-AUC	P-F1	I-AUC	P-F1	I-AUC	P-F1
Un. ³	NOII [21]	0.500	0.157	0.500	0.311	0.500	0.205	0.500	0.124	0.500	0.199
	CFAI [22]	0.482	0.140	0.344	0.320	0.525	0.188	0.500	0.111	0.500	0.190
Full.	Mantra-Net [23]	0.141	0.155	0.701	0.364	0.490	0.286	0.719	0.122	0.513	0.231
	CAT-Net [5]	0.630	0.276	0.782	0.352	0.572	0.134	0.721	0.102	0.693	0.216
	MVSS-Net [6]	0.937	0.452	0.980	0.638	0.731	0.453	0.656	0.260	0.826	0.451
	GSR-Net [24]	0.502	0.387	0.502	0.613	0.515	0.285	0.505	0.175	0.506	0.365
	FCN+DA [1]	0.796	0.441	0.762	0.223	0.541	0.199	0.746	0.270	0.711	0.283
Weak.	MIL-FCN [25]	0.647	0.117	0.807	0.089	0.542	0.121	0.578	0.097	0.644	0.106
	MIL-FCN [25]+WSCL [13]	0.829	<u>0.172</u>	<u>0.920</u>	0.270	0.584	0.178	<u>0.733</u>	<u>0.193</u>	<u>0.766</u>	0.203
	Araslanov and Roth [26]	0.642	0.112	0.773	0.102	0.560	0.127	0.665	0.094	0.660	0.109
	Araslanov and Roth [26]+WSCL [13]	0.796	0.153	0.917	<u>0.362</u>	<u>0.591</u>	0.201	0.701	0.173	0.751	<u>0.222</u>
	Ours	<u>0.816</u>	0.300	0.963	0.382	0.658	<u>0.190</u>	0.783	0.368	0.805	0.310

¹The best and second best results in the weakly supervised method are indicated in **boldface** and underlined, respectively.

²All localization results in **our** method were refined using CGSR.

³Un. means unsupervised methods; Full. means fully supervised methods; Weak. means weakly supervised methods.

TABLE II: Ablation Study of CABL and CGSR Modules on Coverage and IMD2020 Datasets

CABL	CGSR	Coverage		IMD2020		Avg	
		I-AUC	P-F1	I-AUC	P-F1	I-AUC	P-F1
-	-	0.649	0.154	0.767	0.342	0.708	0.248
✓	-	0.658	0.177	0.783	0.361	0.721	0.269
-	✓	0.649	0.175	0.767	0.353	0.708	0.264
✓	✓	0.658	0.190	0.783	0.368	0.721	0.279

TABLE III: Ablation Study of Different CABL Structures on Coverage and IMD2020 Datasets¹

Structure	Coverage		IMD2020		Avg	
	I-AUC	P-F1	I-AUC	P-F1	I-AUC	P-F1
I	0.617	0.130	0.774	0.257	0.696	0.194
II	0.623	0.154	0.767	0.334	0.695	0.244
III	0.658	0.177	0.783	0.361	0.721	0.269

¹All localization results were obtained without CGSR.

volitional features from the prior block, \otimes indicates element-wise multiplication, and \oplus denotes matrix addition.

C. CAM-Guided SAM Refinement (CGSR)

Class Activation Mapping (CAM) [18] is a widely used technique in weakly supervised learning that visualizes regions of an image most influential for classification. Our method enhances CAM maps by fusing convolutional feature maps from the CABL branch with attention weights from the TransBlock [10] (Fig.1), followed by a weighted summation [30]. This combined feature representation is further integrated with the classification head weights of the TransBlock to produce higher-quality CAMs, which serve as coarse-grained masks. The CAM generation process is formalized as:

$$\text{CAM} = \text{CAM}_{\text{Trans}} \cup \left[\frac{1}{L} \sum_l \text{softmax} \left(\frac{Q^l K^{lT}}{\sqrt{D/S}} \right) \otimes \text{CAM}_{\text{Conv}} \right] \quad (2)$$

where $\text{CAM}_{\text{Trans}}$ denotes the CAM [18] generated by the TransBlock, and CAM_{Conv} represents the CAM [18] from the ConvBlock. The symbol \cup represents the union of the two CAM maps, and \otimes indicates element-wise multiplication. Q and K are query and key matrices from the attention mechanism. D is the feature dimension. L is the total number of blocks, and l indexes individual blocks.

However, directly employing these coarse-grained masks as prediction masks may result in incomplete and imprecise localization of the manipulated regions. To address this, we incorporate the Segment Anything Model (SAM) [19], a robust segmentation model that requires no additional training and relies only on the original image and prompts to generate

TABLE IV: Ablation Study of CABL in Different Conv Blocks on Coverage and IMD2020 Datasets¹

Blocks	Coverage		IMD2020		Avg	
	I-AUC	P-F1	I-AUC	P-F1	I-AUC	P-F1
1-4	0.622	0.141	0.727	0.258	0.675	0.200
1-8	0.665	0.125	0.771	0.357	0.718	0.241
1-12	0.658	0.177	0.783	0.361	0.721	0.269

¹All localization results were obtained without CGSR.

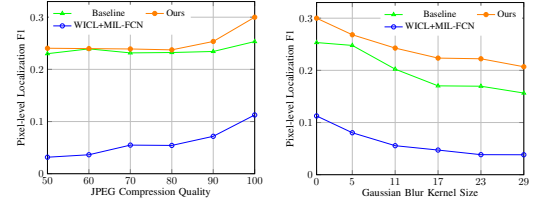


Fig. 5: Robustness Evaluation of JPEG Compression and Gaussian Blur on CASIAv1 Dataset.

accurate segmentation results. As shown in the prompt generator of CGSR in Fig.1, We use the bounding rectangle of the largest connected component in the coarse-grained mask as the bounding box prompt. Additionally, we select one maximum value point (green point in Fig.1) and one minimum value point (red point in Fig.1) from the Class Activation Map (CAM) [18] without maximum-minimum normalization, corresponding to the highest and lowest manipulation probabilities. These two points serve as positive and negative sample point prompts. These prompts are input into SAM to guide precise segmentation. The bounding box and positive point prompts delineate foreground regions, while the negative point suppresses background noise. This combination enables SAM to output high-precision localization maps without further training, effectively resolving boundary ambiguity in the initial CAM predictions.

D. Loss

Our weakly supervised method is trained using only image-level binary classification labels, with the loss function being the sum of the classification losses from the two network branches. The training loss of the model is Eq. (3):

$$\text{loss} = \text{loss}_{\text{CABL}} + \text{loss}_{\text{Trans}} \quad (3)$$

where $\text{loss}_{\text{CABL}}$ and $\text{loss}_{\text{Trans}}$ denote the Binary CrossEntropy Losses (BCE) [28] for the CABL and Trans branches, respectively.

III. EXPERIMENT

A. Implementation details

We trained our model on CASIAv2 [20] using only original images and image-level binary labels, without any pixel-level ground truth. For evaluation, we use CASIAv1 [20], Columbia [10], COVERAGE [31], and IMD2020 [32] to assess both classification and localization. For image-level detection, we report the I-AUC score [1], and for pixel-level localization, we calculate the P-F1 score, following previous methods [13].

The backbone we used is Conformer-S [27], pretrained on ImageNet [33]. The model is trained for 30 epochs with a batch size of 8 using the AdamW optimizer [34], a learning rate of $5e-5$, and a weight decay of $5e-4$. To address the challenges of weakly supervised training (no pixel-level annotations), we applied data augmentation techniques such as random scaling. During inference, multi-scale inputs (256×256, 512×512, and 768×768) were fed into the model, and the resulting predicted maps were aggregated to enhance final localization precision.

B. Comparison with the state-of-the-art methods and Visualization

The Table.I shows that, for image-level manipulation detection, our method achieves the highest average I-AUC among weakly supervised approaches and even outperforms some partially supervised methods. For pixel-level manipulation localization, our method also leads weakly supervised approaches in average P-F1, demonstrating excellent localization performance. While it may not outperform all fully supervised methods, its performance remains comparable to traditional fully supervised techniques. Fig.4 provides visualization examples that illustrate our method’s high accuracy in segmentation and localization. As shown in the fourth row of Fig.4, Our method produces clearer boundaries for the localized manipulated regions compared to the previous weakly supervised method (third row of Fig.4), with a more accurate placement of the manipulated areas.

C. Comparison of Robustness with Weakly Supervised Methods

Following established conventions for evaluating weakly supervised localization robustness [13], we assessed the P-F1 score of manipulated images subjected to JPEG compression with varying compression rates and Gaussian blur with different kernel sizes on CASIAv1 [20]. As shown in Fig.5, our localization method outperforms previous weakly supervised methods [13] in terms of robustness.

D. Ablation Study

1) **Impact of CABL and CGSR Modules on Model Performance:** Ablation experiments on COVERAGE [31] and IMD2020 [32] evaluated the impact of CABL and CGSR modules. Results in Table.II show that CABL alone improves average I-AUC by 0.013 and P-F1 by 0.021 over baseline, while CGSR adds an extra +0.008 to P-F1. The combined modules achieve the highest performance (I-AUC: +0.013,

TABLE V: Ablation Study of **Different Edge Detection Operators in CABL** on Coverage and IMD2020 Datasets¹

Operator	CASIAv1		Columbia		Coverage		IMD2020		Avg	
	I-AUC	P-F1	I-AUC	P-F1	I-AUC	P-F1	I-AUC	P-F1	I-AUC	P-F1
Prewitt	0.824	0.298	0.971	0.113	0.654	0.173	0.761	0.419	0.803	0.251
Sobel	0.816	0.280	0.963	0.302	0.658	0.177	0.783	0.361	0.805	0.280

¹All localization results were obtained without CGSR.

TABLE VI: Ablation Study of **Different CGSR Prompt**

Prompt	CASIAv1 P-F1	Columbia P-F1	Coverage P-F1	IMD2020 P-F1	Avg P-F1
Null ¹	0.280	0.302	0.177	0.361	0.280
Point ²	0.288	0.339	0.176	0.357	0.290
Box ³	0.298	0.359	0.179	0.366	0.301
Box+Point	0.300	0.382	0.190	0.368	0.310

¹Null means no CGSR;

²Point selects the highest probability point from the non-binarized CAM;

³Box selects the largest connected regions in the coarse-grained masks.

P-F1: +0.031 vs. baseline), demonstrating CABL’s role in enhancing region localization accuracy and CGSR’s boundary refinement capability through adaptive prediction optimization.

2) **Ablation Study on Different CABL Structures:** Ablation experiments on COVERAGE [31] and IMD2020 [32] compared three CABL designs (Fig.3) in Table.III. Structure III achieved the highest average classification accuracy and localization precision across both datasets, thus selected as the final configuration due to its superior performance.

3) **Ablation Study on CABL Applied to Different Convolutional Blocks:** Ablation studies in Table.IV compared CABL module application to the first 4, first 8, or all CNN blocks. Applying CABL to all blocks improved average I-AUC by 0.046 (vs. first 4 blocks) and 0.003 (vs. first 8 blocks), with P-F1 gains of 0.069 and 0.028, respectively. This suggests that shallow CABL layers extract texture features, while deeper layers capture high-frequency edge information [6], justifying the full-block implementation.

4) **Ablation Study on Different Edge Detection Operators in CABL:** Ablation experiments in Table.V compared CABL module performance using Prewitt vs. Sobel edge detection operators. The Sobel operator achieved a 0.002 higher average I-AUC and 0.029 higher P-F1 than Prewitt. This is attributed to Sobel’s weighted convolution kernel, which enhances central pixel sensitivity and noise resistance compared to Prewitt’s uniform weights (as analyzed in Sec.II-B). Based on these findings, we adopted the Sobel operator for our CABL module.

5) **Ablation Study on Different Prompts in CGSR:** Ablation experiments (Table.VI) show that combining bounding box and point prompts (with positive/negative point constraints) achieves the best segmentation performance. The CGSR module effectively improves the segmentation accuracy of coarse-grained mask localization.

IV. CONCLUSION

Our proposed framework integrates CABL and CGSR modules for weakly supervised image manipulation localization, achieving state-of-the-art performance in detection and segmentation using only image-level binary labels. The model demonstrates robust generalization across diverse datasets. This work highlights the efficacy of weakly supervised methods for high-fidelity manipulation localization and provides a strong foundation for future advancements in this domain.

REFERENCES

- [1] Xinru Chen, Chengbo Dong, Jiaqi Ji, Juan Cao, and Xirong Li, "Image manipulation detection by multi-view multi-scale supervision," in *ICCV*, 2021, pp. 14185–14193.
- [2] Changtao Miao, Zichang Tan, Qi Chu, Huan Liu, Honggang Hu, and Nenghai Yu, "F2trans: High-frequency fine-grained transformer for face forgery detection," *IEEE TIFS*, vol. 18, pp. 1039–1051, 2023.
- [3] Junke Wang, Zuxuan Wu, Jingjing Chen, Xintong Han, Abhinav Shrivastava, Ser-Nam Lim, and Yu-Gang Jiang, "Objectformer for image manipulation detection and localization," in *CVPR*, 2022, pp. 2364–2373.
- [4] Zenan Shi, Xuanjing Shen, Hui Kang, and Yingda Lv, "Image manipulation detection and localization based on the dual-domain convolutional neural networks," *IEEE Access*, vol. 6, pp. 76437–76453, 2018.
- [5] Myung-Joon Kwon, In-Jae Yu, Seung-Hun Nam, and Heung-Kyu Lee, "Cat-net: Compression artifact tracing network for detection and localization of image splicing," in *WACV*, 2021, pp. 375–384.
- [6] Chengbo Dong, Xinru Chen, Ruohan Hu, Juan Cao, and Xirong Li, "Mvss-net: Multi-view multi-scale supervised networks for image manipulation detection," *IEEE TPAMI*, vol. 45, no. 3, pp. 3539–3553, 2022.
- [7] Yue Wu, Wael AbdAlmageed, and Premkumar Natarajan, "Mantra-net: Manipulation tracing network for detection and localization of image forgeries with anomalous features," in *CVPR*, 2019, pp. 9543–9552.
- [8] Xuntao Liu, Yuzhou Yang, Qichao Ying, Zhenxing Qian, Xinpeng Zhang, and Sheng Li, "Prompt-impl: Image manipulation localization with pre-trained foundation models through prompt tuning," *arXiv preprint arXiv:2401.00653*, 2024.
- [9] Chanda Bhabatosh et al., *Digital image processing and analysis*, PHI Learning Pvt. Ltd., 2011.
- [10] Yu-Feng Hsu and Shih-Fu Chang, "Detecting image splicing using geometry invariants and camera characteristics consistency," in *ICME*. IEEE, 2006, pp. 549–552.
- [11] A Vaswani, "Attention is all you need," *NeurIPS*, 2017.
- [12] Changtao Miao, Zichang Tan, Qi Chu, Nenghai Yu, and Guodong Guo, "Hierarchical frequency-assisted interactive networks for face manipulation detection," *IEEE TIFS*, vol. 17, pp. 3008–3021, 2022.
- [13] Yuanhao Zhai, Tianyu Luan, David Doermann, and Junsong Yuan, "Towards generic image manipulation detection with weakly-supervised self-consistency learning," in *ICCV*, 2023, pp. 22390–22400.
- [14] Yuan Rao and Jiangqun Ni, "A deep learning approach to detection of splicing and copy-move forgeries in images," in *WIFS*. IEEE, 2016, pp. 1–6.
- [15] Yue Wu, Wael Abd-Elmageed, and Prem Natarajan, "Busternet: Detecting copy-move image forgery with source/target localization," in *ECCV*, 2018, pp. 168–184.
- [16] Davide Cozzolino, Giovanni Poggi, and Luisa Verdoliva, "Splicebuster: A new blind image splicing detector," in *WIFS*. IEEE, 2015, pp. 1–6.
- [17] Dianmo Sheng, Dongdong Chen, Zhentao Tan, Qiankun Liu, Qi Chu, Jianmin Bao, Tao Gong, Bin Liu, Shengwei Xu, and Nenghai Yu, "Towards more unified in-context visual understanding," in *CVPR*, 2024, pp. 13362–13372.
- [18] Bolei Zhou, Aditya Khosla, Agata Lapedriza, Aude Oliva, and Antonio Torralba, "Learning deep features for discriminative localization," in *CVPR*, 2016, pp. 2921–2929.
- [19] Alexander Kirillov, Eric Mintun, Nikhila Ravi, Hanzi Mao, Chloe Rolland, Laura Gustafson, Tete Xiao, Spencer Whitehead, Alexander C Berg, Wan-Yen Lo, et al., "Segment anything," in *ICCV*, 2023, pp. 4015–4026.
- [20] Jing Dong, Wei Wang, and Tieniu Tan, "Casia image tampering detection evaluation database," in *CSIP*. IEEE, 2013, pp. 422–426.
- [21] Babak Mahdian and Stanislav Saic, "Using noise inconsistencies for blind image forensics," *IVC*, vol. 27, no. 10, pp. 1497–1503, 2009.
- [22] Pasquale Ferrara, Tiziano Bianchi, Alessia De Rosa, and Alessandro Piva, "Image forgery localization via fine-grained analysis of cfa artifacts," *IEEE TIFS*, vol. 7, no. 5, pp. 1566–1577, 2012.
- [23] Yue Wu, Wael AbdAlmageed, and Premkumar Natarajan, "Mantra-net: Manipulation tracing network for detection and localization of image forgeries with anomalous features," in *CVPR*, 2019, pp. 9543–9552.
- [24] Peng Zhou, Bor-Chun Chen, Xintong Han, Mahyar Najibi, Abhinav Shrivastava, Ser-Nam Lim, and Larry Davis, "Generate, segment, and refine: Towards generic manipulation segmentation," in *AAAI*, 2020, vol. 34, pp. 13058–13065.
- [25] Deepak Pathak, Evan Shelhamer, Jonathan Long, and Trevor Darrell, "Fully convolutional multi-class multiple instance learning," *arXiv preprint arXiv:1412.7144*, 2014.
- [26] Nikita Araslanov and Stefan Roth, "Single-stage semantic segmentation from image labels," in *CVPR*, 2020, pp. 4253–4262.
- [27] Zhiliang Peng, Wei Huang, Shanzhi Gu, Lingxi Xie, Yaowei Wang, Jianbin Jiao, and Qixiang Ye, "Conformer: Local features coupling global representations for visual recognition," in *ICCV*, 2021, pp. 367–376.
- [28] Usha Ruby and Vamsidhar Yendapalli, "Binary cross entropy with deep learning technique for image classification," *IJATCSE*, vol. 9, no. 10, 2020.
- [29] Kaiming He, Xiangyu Zhang, Shaoqing Ren, and Jian Sun, "Deep residual learning for image recognition," in *CVPR*, 2016, pp. 770–778.
- [30] Ruiwen Li, Zheda Mai, Zhibo Zhang, Jongseong Jang, and Scott Sanner, "Transcam: Transformer attention-based cam refinement for weakly supervised semantic segmentation," *JVCI*, vol. 92, pp. 103800, 2023.
- [31] Bihan Wen, Ye Zhu, Ramanathan Subramanian, Tian-Tsong Ng, Xuanjing Shen, and Stefan Winkler, "Coverage—a novel database for copy-move forgery detection," in *ICIP*. IEEE, 2016, pp. 161–165.
- [32] Adam Novozamsky, Babak Mahdian, and Stanislav Saic, "Imd2020: A large-scale annotated dataset tailored for detecting manipulated images," in *WACV Workshops*, 2020, pp. 71–80.
- [33] Jia Deng, Wei Dong, Richard Socher, Li-Jia Li, Kai Li, and Li Fei-Fei, "Imagenet: A large-scale hierarchical image database," in *CVPR*. Ieee, 2009, pp. 248–255.
- [34] I Loshchilov, "Decoupled weight decay regularization," *arXiv preprint arXiv:1711.05101*, 2017.

This figure "fig1.png" is available in "png" format from:

<http://arxiv.org/ps/2503.20294v2>